


Adiabatic population transfer in the D_1 transition of ^{39}K

J. J. Fernández-Soler, J. L. Font, and R. Vilaseca

Departament de Física, Universitat Politècnica de Catalunya, Colom 11, 08222 Terrassa, Spain

 (Received 27 November 2017; revised manuscript received 21 April 2018; published 22 June 2018)

Four-photon stimulated Raman adiabatic passage–like (STIRAP-like) processes in the frame of the D_1 optical transition line of atomic ^{39}K are investigated theoretically by means of a rigorous model that takes into account all the atomic states involved in the interaction with the pump and Stokes light fields and is valid for any field intensities. The same sequential up-down-up-down transition involving two pump (up) and two Stokes (down) photons, going from the initial ground state $|F = 2, M = +2\rangle$ to the final ground state $|F = 1, M = 0\rangle$, which was proven in the past to be very convenient for two-photon amplification and lasing, is considered here. The fact that two atomic states, one with $F = 1$ and another with $F = 2$, participate at each intermediate step of the multiphoton process makes the existence of an ideal unique adiabatic transfer state impossible, and at exact four-photon resonance the population-transfer efficiency to the final atomic state is low (below 60% in general, 80% in the best conditions). Nevertheless, it is shown that by choosing appropriate static detunings for the pump and Stokes fields with respect to the atomic transitions the system follows, sequentially, two adiabatic states, connected by an efficient diabatic passage, so that population-transfer efficiency asymptotically approaching 100% for increasing field amplitudes can be reached. These results are quite robust and suggest the possibility of using STIRAP (or STIRAP-like) pumping to, among other applications, increase the (presently very low) efficiency of two-photon amplification and lasing, a so far unfulfilled goal in quantum and nonlinear optics.

DOI: [10.1103/PhysRevA.97.063848](https://doi.org/10.1103/PhysRevA.97.063848)

I. INTRODUCTION

After more than 25 years from the publication of the paper that presented stimulated Raman adiabatic passage (STIRAP) as a new highly efficient and robust method for population transfer between quantum states [1], progress in the field has been impressive both in the understanding of the process and implementation in different types of systems (including atoms, molecules, solids, superconducting circuits, classical waveguides, etc.) and in the use of STIRAP for a variety of applications, spanning from atomic, molecular, and solid-state physics to quantum information (and even extending to applications in classical physics such as waveguide optics). See, for instance, the recent review of Ref. [2] as well as previous reviews [3–5] and the rest of the references quoted below.

As is well known, in its most standard and conceptually simplest configuration, STIRAP involves only two light fields and three states of the quantum system, with the pump field acting on one of the transitions and the Stokes field acting on the adjacent transition. Nevertheless, for certain applications, in particular in the fields of atom optics and quantum optics (for instance, to transfer a larger momentum from the fields to the atoms or in general to produce a larger change in the state of the quantum system), chain STIRAP (or multiphoton STIRAP) processes involving N quantum states (with $N > 3$) and $N - 1$ photons, each one acting on a consecutive transition in the N -state chain, are more convenient. The efficiency of these processes in transferring the initial-state population to the final or target state, in different interaction conditions, has been investigated or reviewed in, for instance, Refs. [2–4,6–20]. When these processes do not completely fulfill some of the ideal conditions defining a STIRAP process (for instance, when

part of the initial-state population is transiently or permanently transferred to an intermediate state, instead of the target state), these processes are sometimes referred to as STIRAP-like.

The chain or multiphoton STIRAP (or STIRAP-like) processes considered so far, however, have only been implemented, theoretically or experimentally, or exploited, on relatively simple state configurations [2–4,6–21]. For instance, one of the most often considered cases is that where the atomic states participating in the process belong to only two multiplets or levels, which we will refer to as the ground and excited multiplets.¹ In the simplest case, only two fields act on the atoms. For instance, a σ^+ pump beam and a σ^- Stokes beam can take the atoms from an initial state $|g, J = 2, M = +2\rangle$ to a final state $|g, J = 2, M = -2\rangle$ where g (e) denotes the ground (excited) level and J and M are the angular momentum quantum numbers through a four-photon chain (or up-down) process involving an alternate sequence of absorption of a σ^+ photon and emission of a σ^- photon. This configuration has been studied in particular in the case of the optical transition $^3P_2 \leftrightarrow ^3D_2$ of Ne atoms [2,3,6,11,16].

Other similar transitions considered so far are, for instance, $F = 4 \leftrightarrow F' = 4$ and $F = 4 \leftrightarrow F' = 3$, which have been investigated in the D_1 and especially the D_2 lines of cesium [7,8,14,17]. In this case the atom can be adiabatically transferred from state $|g, F = 4, M_F = +4\rangle$ to state $|g, F = 4, M_F = -4\rangle$ through an up-down eight-photon process, using

¹To make sentences more precise, the term multiplet or level will denote the set of atomic quantum states having a definite value of the angular momentum (J or F), whereas the term state or sublevel will denote one specific of these quantum states.

two σ^+ - σ^- polarized fields of the same frequency. All these types of configurations have the advantage that each photon participating in the multiphoton process can be on resonance, or very close to resonance, with its corresponding atomic transition, which can lead to large-population-transfer efficiencies [2,6].

In the case of the D_1 and D_2 lines in alkali-metal atoms, which are very important for atom optics, quantum optics, quantum information, and nonlinear optics and nonlinear dynamics experiments (among other applications), there is the special feature that more than one multiplet exists in both the ground and excited manifolds. Each multiplet corresponds to a different angular momentum number F . The proximity of these additional multiplets to the multiplets that are being considered can affect the multiphoton STIRAP process efficiency, as new quantum channels become open and ac Stark shifts can be induced. In, for instance, the D_1 line of Cs, the separation between the $F' = 4$ and $F' = 3$ multiplets of the excited manifold $2P_{1/2}$ is relatively large (1167 MHz) and thus the perturbation of the eight-photon STIRAP process pointed out above by the presence of the excited level $F' = 3$ is small; theoretical predictions point out 90% adiabatic population-transfer efficiency [14]. For the D_2 line of Cs, however, the hyperfine splittings in the excited-state manifold for the $F' = 5, 4,$ and 3 levels are of only 251 and 201 MHz, respectively, which can reduce the eight-photon STIRAP efficiency to values around 55%, in the best case [7,14,17]. It has also been shown that some part of the population goes to intermediate states, especially to those lying on the ground manifold.

Investigation of multiphoton chain STIRAP processes (i.e., involving more than two photons) in less heavy alkali-metal atoms, where two multiplets can be closer in energy (in the ground and/or in the excited manifolds), is lacking. This is probably due not only to the greater difficulty of the theoretical analysis in those cases, but also to the possible *a priori* belief (induced by results such as those for Cs pointed out above) that the proximity in energy between nearby multiplets will perturb or destroy the adiabatic transfer state and thus will significantly reduce the transfer efficiency for any possible multiphoton STIRAP process (and that introduction of static field detunings [2] could barely counterbalance such a reduction).

This is unfortunate because, as is well known, alkali-metal atoms other than Cs have been, and are being, used frequently for different scientific applications, in particular in the fields pointed out above. One potential specific application, which we are interested in, is that of the implementation of a more efficient two-photon laser. The intrinsic nonlinear nature of the two-photon interaction would make this laser very interesting from quantum and nonlinear dynamics points of view. In fact, since the introduction of lasers, achieving efficient-enough two-photon laser operation has constituted an unfulfilled goal [22–26], which has made experimental study of its singular properties impossible [22,27–36]. The most efficient two-photon laser achieved so far has been one based on an up-down-up-down four-photon process in the D_1 line of potassium (^{39}K), with participation of multiplets $F = 1$ and $F = 2$, in both the ground and the excited manifolds [23]. In the process, two pump (up) photons disappear and, simultaneously, two Stokes (down) photons are created, which amplify the generated laser beam. However, even in this case

the efficiency was very low. We believe that operation of such a class of laser could be significantly improved if a (hopefully efficient enough) four-photon STIRAP-like chain process were used as the pumping-amplifying mechanism, because the high efficiency of the population transfer would entail a high efficiency in the generation of pairs of Stokes photons.

On the basis of these considerations, in this theoretical paper we will consider, essentially, the same four-photon process mentioned above which was used to pump a two-photon laser [23,28], specifically, the process starting at state $|g, F = 2, M = +2\rangle$ and ending at final (target) state $|g, F = 1, M = 0\rangle$ of the D_1 line of ^{39}K , involving absorption of two pump photons and emission of two Stokes, or probe, photons. However, here we will modify the operating conditions (in particular introducing a counterintuitive pulse sequence) in order to favor, if possible, STIRAP or STIRAP-like processes, with the aim of investigating the population transfer efficiency and exploring the best possible operating conditions (leaving application to two-photon laser pumping, or to other potential issues, for subsequent work).

This case is different, with respect to the chain STIRAP configurations investigated so far, that the initial and final states correspond to a different multiplet of the ground manifold (multiplets $F = 2$ and $F = 1$, respectively). From the point of view of a two-photon laser, this must be so in order to have the intermediate steps of the four-photon process out of resonance, avoiding in this way single-photon emissions from these intermediate steps, which could compete with two-photon emission. *A priori*, one would expect that such a feature will make adiabatic transfer less efficient (so far, initial and final states with different angular momentum have only been investigated for three-level systems [37]). However, as it will be shown in this paper, a fortunate participation of an efficient nonadiabatic passage connecting two adiabatic evolutions can strongly increase, in appropriate conditions, global population transfer from the initial to the target atomic state.

The organization of the paper is as follows. In Sec. II the atomic configuration, the multiphoton process to be considered, and the model to study it are established. In Sec. III the obtained results about population transfer are reported, analyzed, and optimized. A summary is given in Sec. IV.

II. ATOMIC CONFIGURATION AND MODEL

In the D_1 line of ^{39}K , the hyperfine splitting within the ground ($4^2S_{1/2}$) and excited ($4^2P_{1/2}$) manifolds is as shown in Fig. 1. The energy separation between multiplets $F = 2$ and $F = 1$ within each manifold is $\Delta_g = 462$ MHz and $\Delta_e = 58$ MHz, respectively. Thus they are so close to each other, in particular in the excited manifold, that one state with $F = 2$ and one state with $F = 1$ will simultaneously participate at each intermediate step of the multiphoton process that we are going to consider [22,29]. Such a multiphoton process, which is depicted in the figure and will be referred to as a $(2 + 2)$ process, involves absorption of two photons from a pump field B and simultaneous emission of two photons from a Stokes field C . We want to transfer as much population as possible from the initial state $|g, F = 2, M = +2\rangle$ (or simply $|g, 2, 2\rangle$)

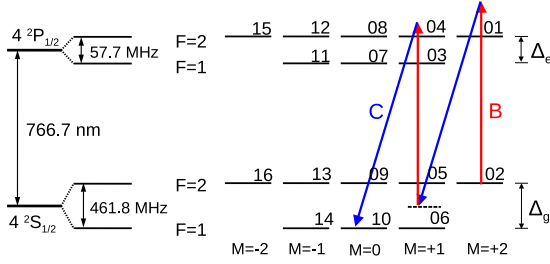


FIG. 1. Atomic energy levels and states for the $^{39}\text{K}D_1$ transition. Note that, to describe specific atomic states, not only will the physical notation $|g, F, M\rangle$ and $|e, F, M\rangle$ be used, but also the simplified sequential notation i , with i going from 01 to 10, just as depicted in the figure. In the dimensionless units that will be defined in the main text, the energy separation between sublevels will be $\Delta_g = 37.43$ and $\Delta_e = 4.68$.

to the final state $|g, F = 1, M = 0\rangle$ (or simply $|g, 1, 0\rangle$), i.e., a state with a different value for both F and M quantum numbers.

The spatial configuration for the light beams is the one depicted in Fig. 2, which, as pointed out above, remains as close as possible to the experimental conditions of the two-photon laser experiments of Ref. [23]. The atomic beam of ^{39}K propagates in the y direction. It is assumed that, before entering the interaction zone with the fields, all atoms have been prepared to be in the initial state $|g, 2, 2\rangle$. A spatial lateral shift of the pump beam B with respect to the Stokes beam C in the y direction, of length δ , is introduced, which will make the atoms interact first with the Stokes beam and then with the pump beam. This defines a counterintuitive interaction sequence, a well-known necessary condition for STIRAP-like population-transfer processes [2] (this lateral shift was not present in the two-photon laser experiments of [23]). The pump field is linearly polarized in the z direction and the Stokes field is σ^- polarized around the z axis, and both fields propagate with constant intensity and Gaussian transverse profile.

If the atoms travel at a certain speed, they will experience the following pulsed fields (expressed in their own reference frame): a pump pulse described as

$$\vec{B}(x, t) = \frac{1}{2} B(t) \vec{u}_z (e^{-i(\omega_B t - k_B x)} + e^{i(\omega_B t - k_B x)}), \quad (1)$$

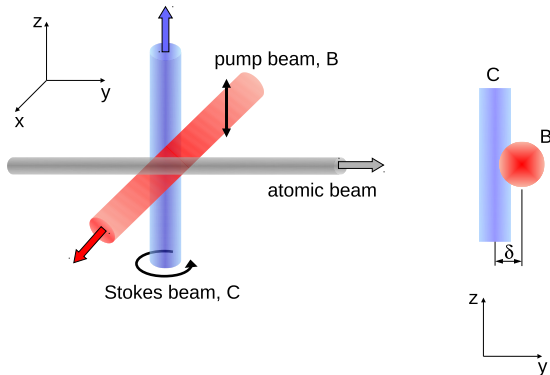


FIG. 2. Geometry (and polarization) of the interacting fields and the beam of ^{39}K atoms.

where \vec{u}_z is a unit vector in the z direction and the amplitude $B(t)$ takes the form

$$B(t) = \tilde{B}_0 \exp \left\{ - \left(\frac{t - t_B}{\sigma_B} \right)^2 \right\}, \quad (2)$$

with σ_B representing the pulse temporal width, and a Stokes pulse given by

$$\vec{C}(z, t) = \frac{1}{2} C(t) (\vec{u}_+ e^{-i(\omega_C t - k_C z)} + \vec{u}_- e^{i(\omega_C t - k_C z)}), \quad (3)$$

where the unit vectors \vec{u} characterize the left-handed polarization and the field amplitude $C(t)$ is given by

$$C(t) = \tilde{C}_0 \exp \left\{ - \left(\frac{t - t_C}{\sigma_C} \right)^2 \right\}, \quad (4)$$

where σ_C represents the pulse temporal width. The temporal delay between the two pulses is $\tau = t_B - t_C$, which is proportional to the beam separation δ . Thus, a positive value of τ will correspond to the counterintuitive sequence characteristic of STIRAP (the Stokes pulse arrives first).

The Stokes field couples with transitions $|e, F, M\rangle \leftrightarrow |g, F', M - 1\rangle$ (Fig. 1) and the pump field interacts with all transitions $|g, F, M\rangle \leftrightarrow |e, F', M\rangle$, for any allowed value of F , F' , and M . In the usual rotating-wave and slowly varying envelope approximations, the semiclassical density-matrix equations describing the atomic state can be expressed as

$$\begin{aligned} \dot{\sigma}_{ii}(t) &= \lambda_i - (\gamma_i + \gamma_{\text{int}}) \sigma_{ii}(t) - \sum_{j \neq i} \gamma_{ji} \sigma_{ij}(t) \\ &+ \sum_{j \neq i} \gamma_{ji} \sigma_{jj}(t) + F_{ii} \{ \sigma_{ij}(t), B_{ij}(t), \\ &\times C_{ij}(t), \Delta_B, \Delta_C \}, \end{aligned} \quad (5a)$$

$$\begin{aligned} \dot{\sigma}_{ij}(t) &= -\Gamma_{ij} \sigma_{ij}(t) + F_{ij} \{ \sigma_{ii}(t), \sigma_{ij}(t), B_{ij}(t), \\ &\times C_{ij}(t), \Delta_B, \Delta_C \}, \end{aligned} \quad (5b)$$

where the density-matrix elements ρ_{ii} and ρ_{ij} have been expressed as

$$\rho_{ii}(t) = \sigma_{ii}(t), \quad (6a)$$

$$\rho_{ij}(t) = \sigma_{ij}(t) e^{-i[n(\omega_C t + \phi_C) - m(\omega_B t + \phi_B)]}, \quad (6b)$$

so σ_{ii} and σ_{ij} represent the population of state $i = |a, F, M\rangle$ (with a denoting g or e) and the slowly varying envelope of the atomic coherence induced on the transition between states i and j , respectively [n and m represent the number of Stokes and pump photons, respectively, of the $(m + n)$ -photon transition connecting both states]. The term λ_i gives the rate of injection of atoms with internal state i into the region of interaction with the pulses. The parameter γ_{int} is the inverse of the total interaction time of the atoms with the fields considered in each calculation, t_{int} .

The functions F_{ii} and F_{ij} arise from the quantum Liouville evolution commutator and represent the effect of the fields on the atomic state. They depend on, among other parameters, the Rabi frequencies associated with the different fields and transitions (for further details see [28,38])

$$2B_{ij}(t) = \frac{\mu_{ij} B(t)}{\hbar}, \quad 2C_{ij}(t) = \frac{\mu_{ij} C(t)}{\hbar}, \quad (7)$$

where $2B_{ij}(t)$ [$2C_{ij}(t)$] is the Rabi frequency for the pump (Stokes) field when interacting with a transition between atomic states i and j and $\mu_{ij} = \mu_0 \chi_{ij}$ is the electric dipole matrix element of the transition (see [38] for a detailed discussion about its calculation and value, for each transition; $\mu_0 = 3.507 \times 10^{-29}$ C m is a reference value and χ_{ij} is a Clebsch-Gordan-related factor specific to each transition). On the other hand, in the results below the peak field amplitudes will be expressed by means of the normalized quantities $B_0 = \mu_0 \tilde{B}_0 / 2\hbar$ and $C_0 = \mu_0 \tilde{C}_0 / 2\hbar$.

The detuning of the pump (or drive) field with respect to the optical transition is controlled by the parameter $\Delta_B = \omega_B - \omega_{e2-g1}$, where ω_{e2-g1} is the frequency of the transition $|e, 2, M\rangle \leftrightarrow |g, 1, M\rangle$ for any M , whereas $\Delta_C = \omega_C - \omega_B$ controls the difference between the Stokes (or probe) and pump field frequencies. Note that the global detuning of the $(2+2)$ four-photon process for the bare atom is $\Delta_{(2+2)} = \Delta_C - \Delta_g/2$.

The relaxation mechanisms (spontaneous emission and collisions) are characterized by γ_i and γ_{ij} for the populations and by Γ_{ij} for the coherences. Nevertheless, throughout all our calculations we have set all these relaxation terms equal to zero. Thus, the only mechanism left for population transfer between atomic states is the coherent interaction with the two fields, so the final population in the target state becomes a direct measurement of the efficiency of the STIRAP process under study. In fact, as it will be discussed later, in conditions of an efficient STIRAP-like process only a very small part of the population will transiently visit the excited states, so spontaneous emission should not be expected to play a significant role. Moreover, in our case, by increasing the atomic velocity and reducing the beam cross sections the interaction time of the atoms with the fields could be made as short as possible, so the probability for spontaneous emission processes to take place during the interaction time could be reduced. On the other hand, the use of an atomic beam greatly diminishes the collisions among atoms and the population transfers they could lead to.

Finally, throughout the paper, all quantities with dimensions of s^{-1} (including B_0 and C_0) have been converted to dimensionless form by normalizing (dividing) them by $\Lambda = 7.75 \times 10^7 s^{-1}$ (see [38]). Consistently, quantities with dimensions of s have been multiplied by Λ [38].

III. RESULTS

In our work, and as usual in STIRAP studies [2], two main complementary tools have been used: numerical integration of Eqs. (5) and calculation of the instantaneous eigenvalues and eigenvectors of the Hamiltonian of the system. In order to better understand the dynamics of the population-transfer process in such a complex atomic system, we first considered truncated atomic models, in which several of the 16 atomic states of Fig. 1 have been ignored. This has provided valuable information, which is summarized in the following section.

A. Results for truncated-system models

When only five atomic states are considered, in such a way that only one state for each intermediate step of the $(2+2)$ four-photon process (Fig. 1) is taken into account and states

11–16 (in the simplified notation of that figure) which lie beyond target state 10 are ignored, then the STIRAP process works very well. We mean that when the $(2+2)$ multiphoton process is on exact resonance $\Delta_{(2+2)} = 0$ (a well-known necessary condition for efficient adiabatic transfer in this type of configuration [2]), the maximum population transfer from initial state 02 to target state 10 always occurs for pulse delay values around $\tau = 1$ (especially in the cases with greater efficiency) and the efficiency grows monotonically toward 100% with increasing fields amplitude, as shown in Fig. 3(a). These are typical signatures of STIRAP (or STIRAP-like) processes [2]. We interpret that this occurs because the mathematical condition for the existence of an adiabatic-passage

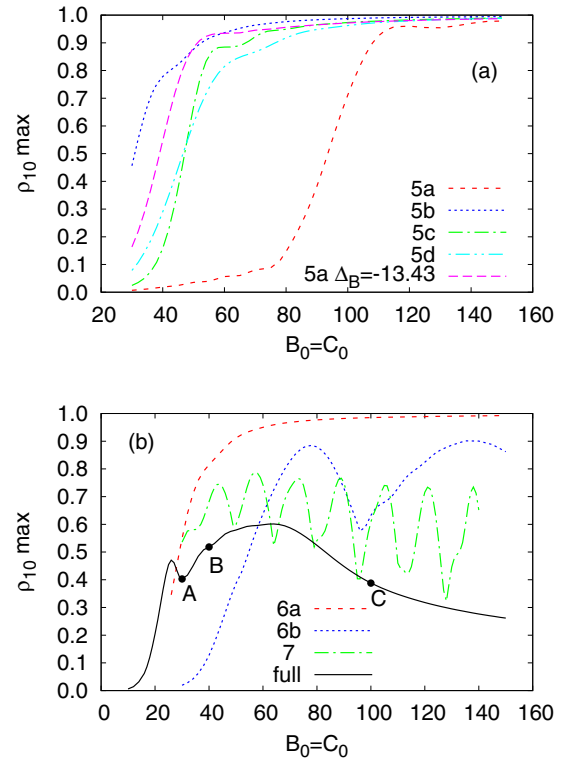


FIG. 3. (a) Efficiency curves (population transferred to the target state vs amplitude of the two fields) obtained for the four possible truncated five-state models. Here $\rho_{10 \text{ max}}$ represents, for each point of the curves, the maximum population reached by target state 10 (in the notation of Fig. 1) at the end of the interaction with the two pulses, after scanning for different values of the pulse delay τ . All these truncated models exclude atomic states 09 and 11–16 and include states 01, 02, and 10. The rest of the states included in each model are, for model 5a, 04 and 05; for model 5b, 04, and 06; for model 5c, 03 and 05; and for model 5d, 03 and 06. In all cases the parameters are $\sigma_B = \sigma_C = 1$, $\Delta_{(2+2)} = 0$, and $\Delta_B = -\Delta_g = -37.43$ (i.e., the resonance of the pump field with respect to the transition $02 \leftrightarrow 01$), except for the last curve, for which $\Delta_B = -13.43$ (to show that changing the pump field detuning does not qualitatively change the results but can optimize the efficiency). (b) Same as in (a), for truncated models with six or seven atomic states and for the full model with the 16 atomic states. Models 6a and 6b are like models 5a and 5c, respectively, but also include state 06. Model 7 is like model 6a but also includes state 03. Points A, B, and C of the full-model curve correspond to $B_0 = C_0 = 30, 40, 100$, respectively, and will be considered in the main text.

state, involving detunings and Rabi frequencies, derived in [18] (see also [2,39]), is fulfilled in our case (except, in some of the cases, for small field amplitudes). Calculation of the five eigenvalues and eigenvectors of the corresponding time-dependent Hamiltonian supports this conclusion, in the sense that the system follows quite closely an eigenvector that starts at initial atomic state 02 and ends at target state 10. The total population that transiently stays at intermediate excited states 01, 03, and 04 reaches a peak of only approximately 2%, and the population transiently going through ground intermediate states 05 and 06 reaches a peak of approximately 20% (results are omitted for the sake of brevity), which is also compatible with previous theoretical modeling of other five-state atomic systems [2,18,39].

However, when one further atomic state is considered in the intermediate steps of the $(2 + 2)$ four-photon process (i.e., when truncated six-state models are considered), the STIRAP signatures are lost in some conditions, as shown in Fig. 3(b). As it can be seen, model 6a continues to be efficient, but for model 6b the monotonic growth with field amplitude is lost and the transfer curve shows some wide oscillations never reaching 100% efficiency. We have found that this occurs because of a nonconstructive interference between two parallel quantum channels within the $(2 + 2)$ four-photon process: channels $01 \leftrightarrow 05 \leftrightarrow 03$ and $01 \leftrightarrow 06 \leftrightarrow 03$. Analysis of the Clebsch-Gordan coefficients of the involved transitions [38] indicates that this occurs because these two parallel $(1 + 1)$ segments of the four-photon process do not fulfill the so-called proportional couplings condition [39] required for $(1 + 1)$ processes that involve more than one state at the intermediate step of the process (see also [2,40–42]). According to [39], the efficiency could still be high for some particular values of the detunings, but we have not investigated such a possibility.

Including still one further atomic state in the model so that all the states lying between the initial state 02 and target state 10 are considered (thus leading to a truncated seven-state model) makes a few additional quantum channels also participate in the process. We have detected further interference effects between these channels, which also negatively affect the population-transfer efficiency to the target state, leading to tighter oscillations on its dependence on the fields amplitude, as shown in Fig. 3(b).

B. Full-system model

Finally, when all 16 atomic states are taken into account (i.e., also including state 09 and states 11–16 lying beyond target state 10, Fig. 1) and the $(2 + 2)$ four-photon process is kept on exact resonance, the transfer efficiency further decreases, as shown in Fig. 3(b). A maximum transfer efficiency of about 60% is reached, which monotonically decreases at larger field amplitudes, instead of continuing to increase. We interpret that this further deterioration is mostly due to the large ac Stark shifts induced by the presence of all these extra states on the states that directly participate in the different steps of the $(2 + 2)$ four-photon process and especially on target state 10. These ac Stark shifts put the $(2 + 2)$ four-photon process increasingly out of resonance when the field amplitudes increase, making it progressively less efficient. A qualitatively similar behavior was already found in other multiple-intermediate-

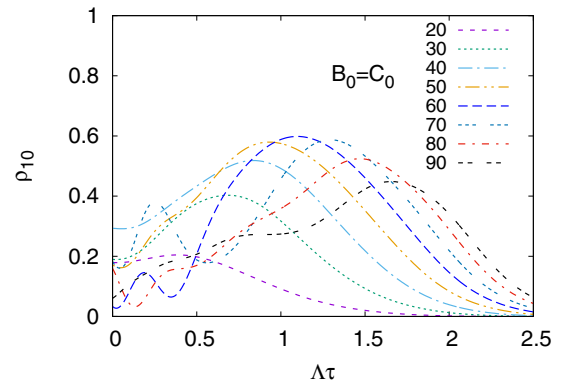


FIG. 4. Final population in target state 10 as a function of the time delay τ between Stokes and pump pulses, for different values of the field amplitude (considered equal for both pulses), with the full model.

state systems [2,4,5,37,39,43–45]. The extra states that exist beyond the target state 10 (Fig. 1) could also eventually take up part of the population (reducing the efficiency of population transfer to the target state), but in fact for large field amplitudes they only capture a very small fraction of population (as it will be seen in curves below), as these states are out of resonance of all possible multiphoton transitions.

Such deviation from ideal STIRAP behavior is also noticeable when looking at the dependence of the population-transfer efficiency on the time delay τ between Stokes and pump pulses, as shown in Fig. 4. It can be seen that, in contrast to an ideal STIRAP case, maximum population-transfer efficiency is not always found at $\tau = 1$ (even for the largest field amplitudes, for which adiabaticity should be favored), but at some other value, although not far from it. Also, there is no clear wide plateau around the maximum value, although the dependence on τ is smooth.

To complete the description of the full-model results, Fig. 5(a) shows the temporal evolution of the four most relevant eigenvalues of the instantaneous Hamiltonian of the system, for point B of Fig. 3(b) (see the figure caption for further details about these eigenvalues). Figure 5(b) shows the projection of the exact instantaneous atomic state (i.e., the Bloch vector) on all 16 eigenstates of the system (in particular on the four eigenstates corresponding to the previous four eigenvalues). There is no eigenstate starting at the initial atomic state 02 and ending, after the interaction with the Stokes and pump pulses, the at target state 10). As it can be seen, the system, which initially is at atomic state 02, starts on a balanced linear combination of eigenvectors e_{13} and e_{15} . At $t = 2.8$ there is a physically irrelevant anticrossing (avoided crossing) with a very small gap, imperceptible in Fig. 5(a), which is diabatically and efficiently crossed by the system so that, formally, its component on e_{15} suddenly changes to e_{14} . The projection on this eigenvector grows progressively, but from $t \simeq 5.5$ to $t \simeq 6.0$ it rapidly decreases down to a value of approximately 60% at the same time that a projection of approximately 32% on e_{15} appears. This mixing is due to the wide-gap anticrossing between e_{14} and e_{15} which appears in Fig. 3(a) for that range of time. We have checked that e_{14} , from $t = 5$ to $t = 8$, takes a

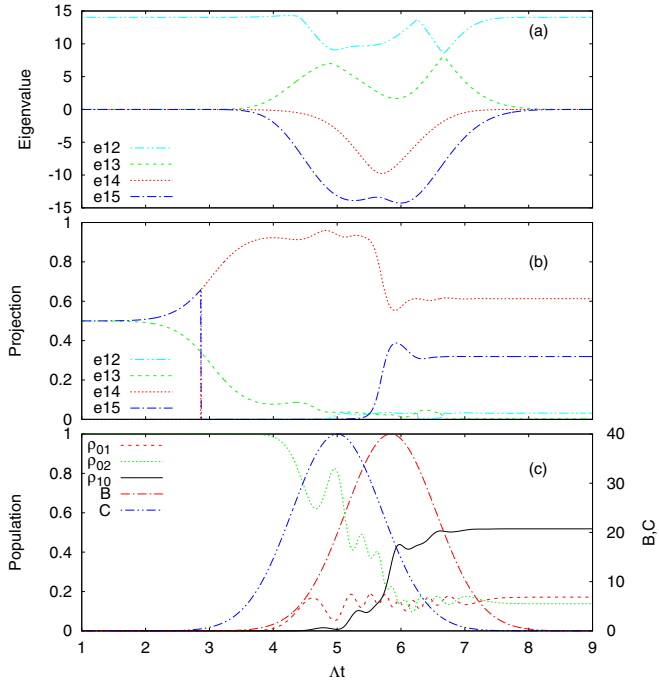


FIG. 5. For point B of Fig. 3(b). (a) Temporal evolution of four of the 16 Hamiltonian eigenvalues of the full model (as usually done, eigenstate numbers have been ordered, at each time t , from largest to smallest energy value). At the initial and final times, eigenstate e_{12} coincides with atomic state 03, eigenstates e_{13} and e_{15} are a 50%-50% linear combination of states 01 and 02, and e_{14} coincides with state 10 (no eigenstate starts at initial atomic state 02 and ends at target state 10). (b) Temporal evolution of the projection (square of the component) of the atomic state on each one of the 16 eigenstates of the system, in particular on e_{12} – e_{15} . (c) Temporal evolution of the atomic state populations. Also depicted is the temporal profile of the two pulses $B(t)$ and $C(t)$ (right vertical axis).

growing component on target atomic state 10 (going from 0% to 100%). All this clearly explains the temporal evolution of atomic state populations shown in Fig. 5(c), in particular the moderate growth of the population of target state 10 [and also, similarly, in Fig. 8 below, for points B and C of Fig. 3(b)].

In summary, two concomitant causes have been found as responsible for the relatively low efficiency of the full model. First, there is at least one quantum channel in the $(2 + 2)$ multiphoton process which does not fulfill the proportional couplings condition and thus negatively interferes with another channel. Second, the atomic states other than those directly involved in the $(2 + 2)$ four-photon process induce ac Stark shifts which take the process out of resonance.

C. Optimization and robustness

We have further explored the parameter space to find whether conditions exist for which the population-transfer efficiency is larger and grows with increasing field amplitude (asymptotically approaching, if possible, 100%). Note that the only parameter that has been scanned so far, for each point on the curves of Fig. 3, is, as pointed out above, the pulse delay τ . We have now scanned further parameters, in the following way.

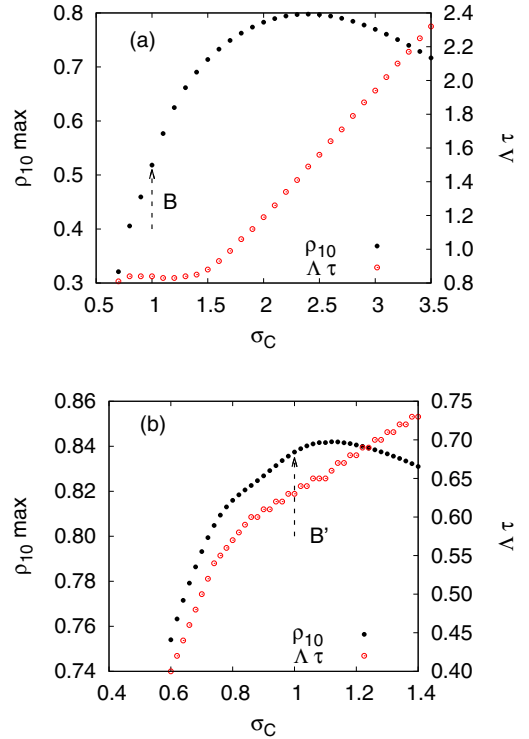


FIG. 6. (a) Final population transferred to target state 10 (left vertical axis) and corresponding optimal value of the pulse delay τ (right axis), as a function of the temporal width of the Stokes pulse σ_C (σ_B remains equal to 1). For $\sigma_C = 1$ it corresponds to point B of Fig. 3(b). The rest of the parameters are the same as in that figure. (b) Same as (a) for optimized point B' of Fig. 7 below.

In a first exploration, the field detunings have been kept fixed to the previous values. In particular, the $(2 + 2)$ four-photon process has continued to be on resonance, $\Delta_{(2+2)} = 0$. In such conditions, it has been found that the relative amplitude of the two pulses does not play a key role, as its variation only leads to small improvements or, more often, deteriorations of the transfer efficiency. The relative temporal width of the pulses, however, has a relatively larger influence: Making $\sigma_C > \sigma_B$ leads, for many of the points of the full-model curve in Fig. 3(b), to a more significant increase in the transfer efficiency, as shown in Fig. 6(a) for the particular case of point B of Fig. 3(b). As it can be seen, increasing σ_C from 1 to 2.4 increases the transfer efficiency from 52% to 80%. The temporal evolution of the eigenvalues (not shown for the sake of brevity) is qualitatively similar to that of Fig. 5(a), with again no eigenvector starting at the initial atomic state 02 and ending at the target state 10. However, now, with larger σ_C , the narrow-gap anticrossing between e_{14} and e_{15} appearing at an early time shifts to much later times, so the system starts on eigenvector e_{14} (which now initially coincides 100% with atomic state 02 and will take an increasingly large component on target state 10) and remains with a very large projection on it (above 90%) for most of the time. The wide-gap anticrossing between e_{14} and e_{15} pointed out above continues to appear, in time, at the middle of the interaction, but now it is wider and thus the atomic state only takes a small component over e_{15} . Finally, at the small-gap anticrossing appearing near the end of

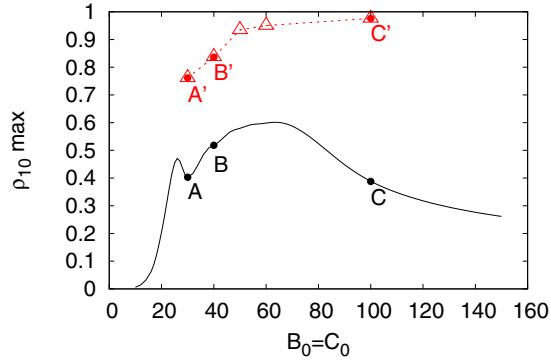


FIG. 7. Final population transferred to target state 10 as a function of the peak amplitude of the pump and Stokes pulses (considered equal) for the full model. In black, the nonoptimized efficiency curve of Fig. 3(b) is reproduced. Red triangles show the values achieved using the detunings obtained after the optimization procedure described in the main text (as the procedure is lengthy, only five points have been calculated; the red line is only a guide for the eye). Particular points labeled A , B , C , A' , B' , and C' are analyzed in the main text. The rest of the parameters are as in previous figures and in Table I.

the pulses the system sharply jumps diabatically and efficiently to eigenvector e_{15} (which ends up with 100% component on target atomic state 10).

Nevertheless, keeping $\Delta_{(2+2)} = 0$, we have not found results significantly better than these. In particular it is difficult to find a monotonic growth of the population-transfer efficiency with increasing fields amplitude. Thus, in a second exploration

TABLE I. Maximum final population in target state 10, time delay τ , and detunings $\Delta_{(2+2)}$ and Δ_B corresponding to each one of the points obtained by means of the optimization procedure (red triangles in Fig. 7).

$B_0 = C_0$	Final population	τ	$\Delta_{(2+2)}$	Δ_B
30	0.7616	0.33	1.5	-42
40	0.8374	0.63	4.0	-43
50	0.9348	0.21	3.0	-84
60	0.9504	0.13	3.4	-115
100	0.9760	0.43	4.7	-250

in the parameter space, we have also varied the $(2+2)$ four-photon detuning $\Delta_{(2+2)}$ and the pump detuning Δ_B . In fact, in other works about STIRAP (dealing in general with only a three-level system, but with more than one intermediate state or involving a hyper-Raman process), it was found that introducing static detunings in the intermediate single-photon steps of the multiphoton (two-photon, in those cases) process could counterbalance, to some degree, the two causes of efficiency loss mentioned above, destructive quantum-channel interference and ac Stark shifts [2,5,37,39,42–44,46], although in those cases only one of the two types of cause, but not both simultaneously, was present (some other technique has also been proposed, such as chirped, or Stark-chirped, rapid adiabatic passage [5,47–49], but it would require a more complex light-matter configuration).

These two detunings have been scanned following an optimization procedure consisting in, starting with a fixed value

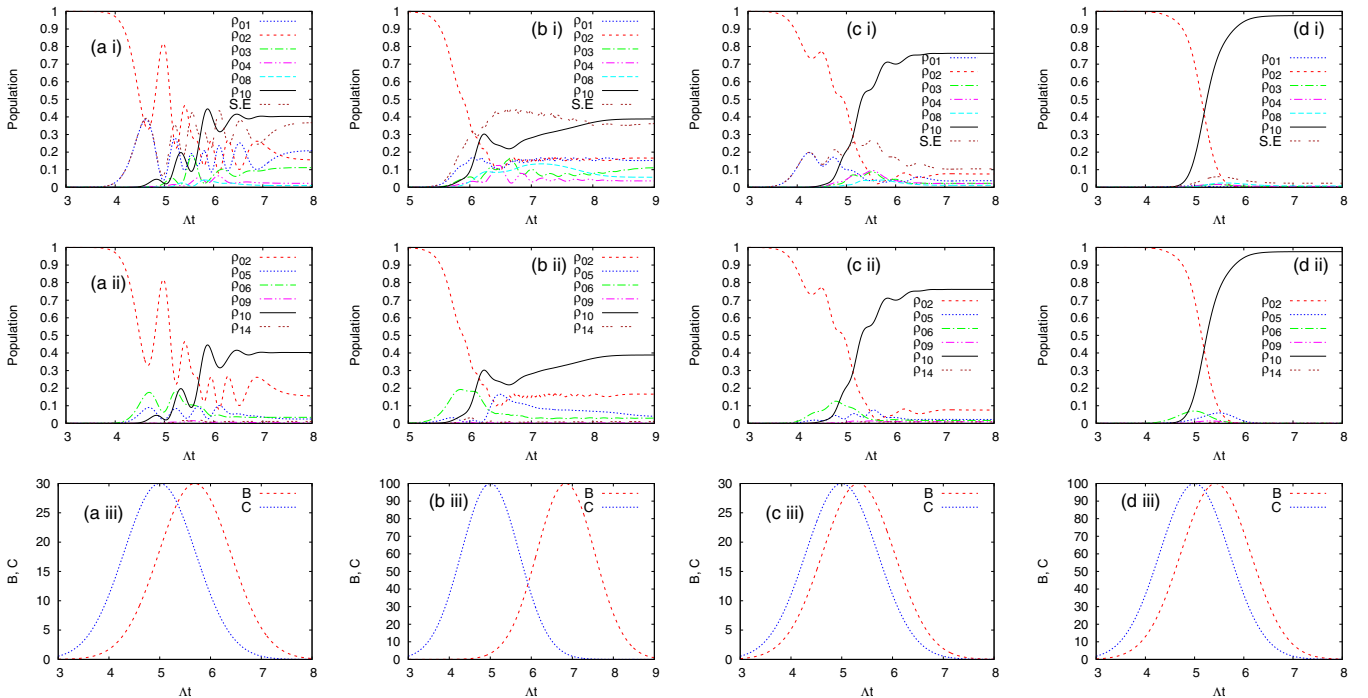


FIG. 8. Time evolution of the fields and the most significant populations, for the following points of Fig. 7: (a i), (a ii), and (a iii) point A (the curve labeled S.E. corresponds to the sum of the populations in all the atomic states of the excited manifold); (b i), (b ii), and (b iii) point C ; (c i), (c ii), and (c iii) point A' ; and (d i), (d ii), and (d iii) point C' . The top row contains populations of excited-manifold states and also, for comparison, of the initial 02 and target 10 states. The middle row only contains populations of ground-manifold states. The bottom row shows, as a reference, the temporal profile and delay of the two pulses, for each case.

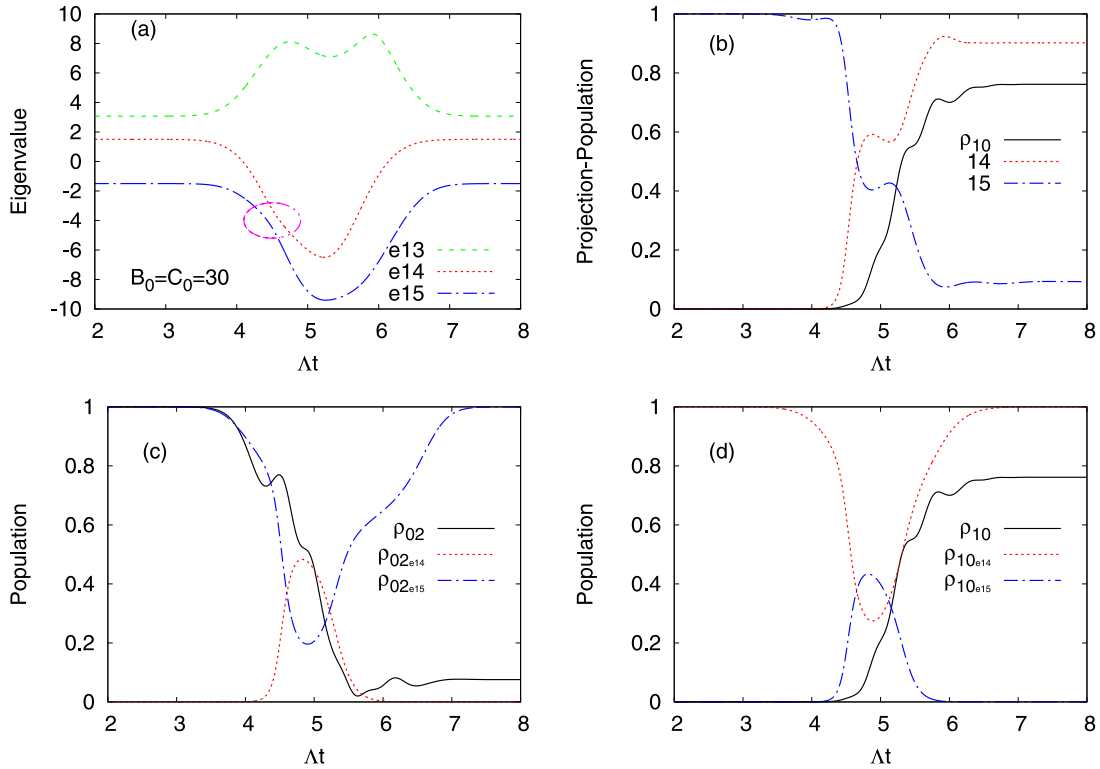


FIG. 9. (a) Time evolution of the three most relevant Hamiltonian eigenvalues, denoted by e_{13} , e_{14} , and e_{15} , corresponding to optimized point A' of Fig. 7. The zone of the avoided crossing, i.e., where eigenvalues e_{14} and e_{15} get close enough to allow the system to jump from eigenstate e_{15} to eigenstate e_{14} , are marked with a circle. (b) Projection (square of the component) of the system state (Bloch vector) on eigenvectors e_{14} (red dotted line) and e_{15} (blue dash-dotted line) and population of target state 10 (black solid line). (c) Projection of eigenvector e_{14} of (a) over initial state 02 (the black solid line shows, as a reference, the population of this state). (d) Projection of eigenvector e_{15} over target state 10.

of Δ_B , varying $\Delta_{(2+2)}$ to determine the value that optimizes the transfer efficiency; then, fixing this $\Delta_{(2+2)}$ value, Δ_B has been varied to find a new optimum; next, starting with this last value, the whole process has been repeated, and so on. As before, for each particular set of parameters the time delay τ has been scanned in order to select the value that maximizes the population transfer. On the other hand, in order to facilitate comparisons, the pulse width of both pulses has been kept equal to 1 (its influence has been studied in a subsequent step).

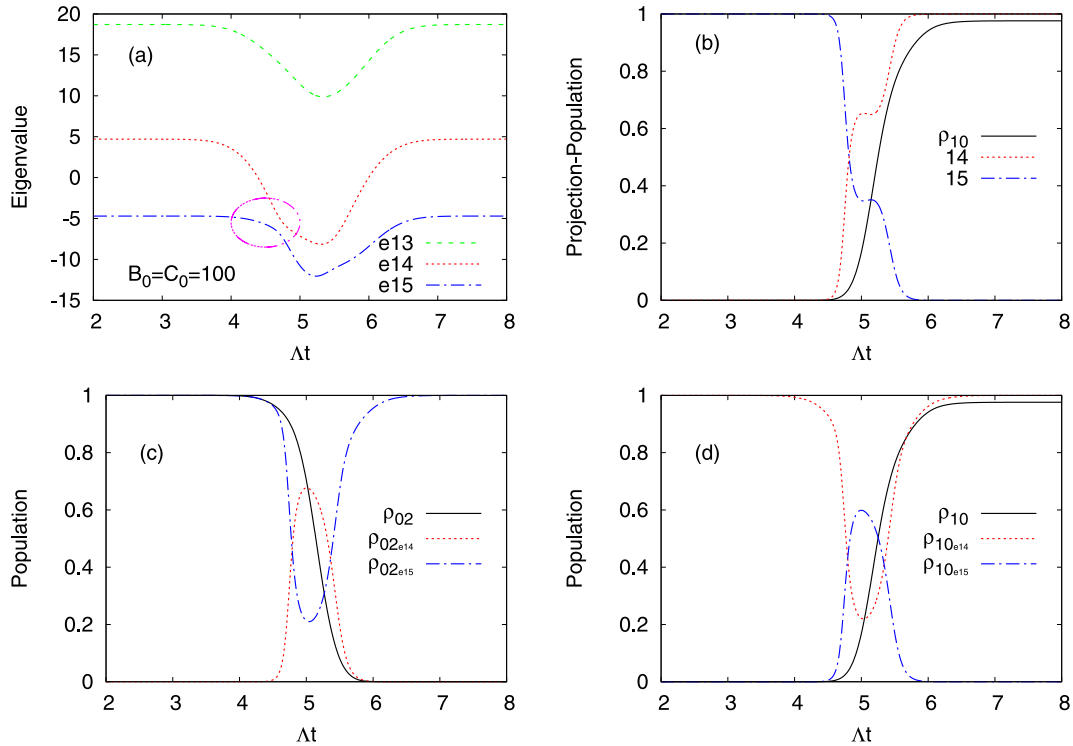
Figure 7 shows the result of this optimization procedure. The lowest (black) curve reproduces the nonoptimized efficiency curve of Fig. 3(b) for the full model, for the original values of $\Delta_{(2+2)}$ and Δ_B . In contrast, the red triangles indicate the values obtained for the final population in target state 10 after the optimization process. The values of τ , $\Delta_{(2+2)}$, and Δ_B corresponding to these optimized points are given in Table I.

It is clear that the optimized results are remarkably (and perhaps surprisingly) good. The efficiency so obtained shows a definite tendency to increase, approaching a 100% value when the pulses amplitude grows.

This conclusion is also confirmed by inspection of the temporal evolution of the atomic states populations, as Fig. 8 shows. Figures 8(a) and 8(b), which correspond to points A and C , respectively, of Fig. 7, confirm what was already found for Fig. 5 (where point B was considered): Before the optimization, the population transfer does not take place in a monotonically growing and efficient way from the initial state

to the target one. Instead, a series of step-by-step processes and Rabi oscillations take place [compare, for instance, the time evolution of populations in states 01 and 02 and also (less noticeable) those in states 02 and 06, in Fig. 8(a)]. These figures also show that a significant population (40% of the total) goes to excited atomic states instead of the target state 10. In contrast, for points A' and C' [Figs. 8(c) and 8(d), respectively] obtained through the optimization procedure, the population transfer is more direct and efficient and monotonically grows with field amplitude. Especially with the highest amplitude (point C'), no Rabi oscillations take place and the excited-manifold states are sparsely populated [notice in Fig. 8(d) i) that the total population of all atomic states lying at the excited manifold reaches a transient peak value of only approximately 3%].

To understand why this efficiency improvement occurs, Figs. 9 and 10 summarize the eigenstates behavior for optimized points A' and C' , respectively, of Fig. 7. For both points, as the system is out of $(2+2)$ four-photon resonance, the degeneracy between Hamiltonian eigenvalues at both initial and final times is removed [Figs. 9(a) and 10(a)]. There is again no pure adiabatic-transfer state connecting the initial and target atomic states: Eigenstate e_{15} starts 100% at the initial state 02 [Figs. 9(c) and 10(c)], whereas e_{14} ends 100% at the target state 10 [Figs. 9(d) and 10(d)]. Nevertheless, at a certain moment these two eigenvalues come close together [Figs. 9(a) and 10(a), indicated by a circle], defining an avoided crossing where the system can diabatically jump from one eigenvector


 FIG. 10. Same as in Fig. 9 for point C' of Fig. 7.

to the other with high efficiency. Thus what happens is that the atomic system starts by adiabatically following eigenstate e_{15} and at the avoided crossing it passes diabatically, in large measure, to eigenstate e_{14} , continuing with a very large component on it until the end of the interaction [Figs. 9(b) and 10(b)]. This diabatic passage is more complete or efficient for point C' than for point A' , in principle due to the larger amplitudes of the two fields in this case. In effect, for point C' Fig. 10(b) shows that 97% of the atoms reach target state 10 and that the Bloch vector of the system follows very closely the first eigenvector e_{15} and the next eigenvector e_{14} . In contrast, for point A' [Fig. 9(b)], the efficiency is only of approximately 76% and the Bloch vector keeps a larger (but still moderate) component on other eigenstates, in particular on e_{13} and e_{15} . As a last remark, it is also worth noting that the passage from e_{15} to e_{14} does not exclusively occur at the anticrossing point indicated just above; inspection of Figs. 9(a), 9(b), 10(a), and 10(b) shows that, indeed, the passage takes place mostly there, but in fact it is completed a few instants later. This is because, after the anticrossing, eigenvalues e_{14} and e_{15} still remain relatively close to each other, for a certain period of time, and it even seems that they define another, weaker, anticrossing, with a larger gap [barely perceptible in Figs. 9(a) and 10(a), somewhat more apparent in Figs. 12(a) and 12(c) below].

The participation of efficient diabatic passage through an avoided crossing has also been reported in other cases of STIRAP or STIRAP-like processes (usually in three-level systems), in particular when the fields are out of resonance (especially out of two-photon resonance) and/or when there is more than one state in the intermediate step of the process [2,4,5,37,39,44,45,45,50].

As pointed out above, the results of the upper curve of Fig. 7 have already been optimized with respect to pulse delay τ , pump detuning Δ_B , and four-photon detuning $\Delta_{(2+2)}$. Figure 11 clearly illustrates that for point B' . It is worth noting that increasing τ above 0.63 (which is the value for point B') reduces the gap of the anticrossing between eigenvalues e_{14} and e_{15} and in principle this should help the transfer process. For instance, when going from $\tau = 0.63$ (point B') to $\tau = 1.09$ [Figs. 12(a) and 12(c), respectively], that gap reduces from approximately 1.4 to 0.12 (it appears in these figures at $\Delta t \simeq 4.6$). With such a small gap, the diabatic passage from e_{15} to e_{14} there is faster and highly efficient [Fig. 12(d)]. However, the second (wider) anticrossing pointed out above, which appears at a slightly later time [it appears at $\Delta t \simeq 5.3$ in Fig. 12(c)], becomes now better defined (the gap decreases) and inverts the process; i.e., it makes the Bloch vector take again a large component (slightly above 50%) over e_{15} , as shown in Fig. 12(d). This is the main reason why larger values of τ are not more efficient. Let us point out here that the two other anticrossings appearing in Figs. 12(a) and 12(c) because of the proximity, in this case, of eigenvalue e_{13} to eigenvalue e_{14} do not play any physical role, because the first of them does not affect the atomic state and the second has such an extremely narrow gap that the system crosses it diabatically with complete efficiency.

The results of the upper curve of Fig. 7 could still be further optimized to some degree by scanning the Stokes pulse duration σ_C . Nevertheless, the value used for the points of that curve ($\sigma_C = 1$) is already close to the optimum value, as it can be seen in Fig. 6(b) above, as increasing σ_C above unity (the value corresponding to point B') can only lead to a transfer

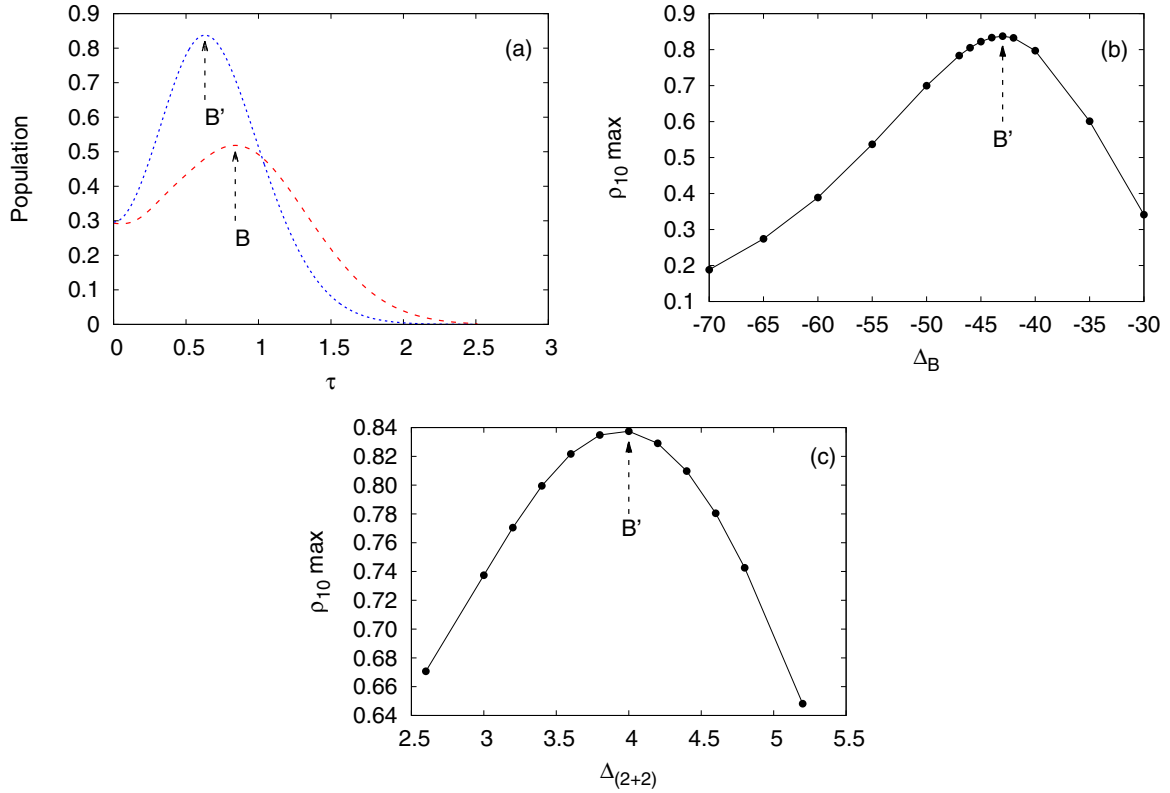


FIG. 11. Final population in target state 10 (a) as a function of the pulse delay τ , for values around point B (lower curve) and point B' (higher curve) of Fig. 7, (b) as a function of pump detuning Δ_B , for values around point B' of Fig. 7, and (c) as a function of the $(2 + 2)$ four-photon process detuning $\Delta_{(2+2)}$, also for values around point B' of Fig. 7. In all cases the rest of the parameters are as in Fig. 7.

efficiency improvement of approximately 0.7% (reached for $\sigma_C = 1.12$). In this figure, the efficiency growth with σ_C (for $\sigma_C < 1.12$) is mainly due to the fact that the e_{14} - e_{15} anticrossing gap monotonically decreases with increasing σ_C , which helps diabatic passage. In addition, the efficiency decline for larger σ_C is mainly due to the growth of the gap of the second anticrossing between e_{13} and e_{14} [Fig. 12(a)], which for large enough σ_C starts to play a role in making progressively less efficient the diabatic passage through it.

Finally, Figs. 6(b) and 11 also illustrate the significant robustness of the optimized results with respect to variations in the different system or control parameters. As it can be seen, none of the parameter values is critical. The highest sensitivity is with respect to variations of the $(2 + 2)$ four-photon detuning $\Delta_{(2+2)}$ [Fig. 11(c)], as would also be the case even for an ideal STIRAP process in a three-level atom, and the pulse delay τ [Fig. 11(a)], where it can be seen that the sensitivity is larger for optimized point B' than for nonoptimized point B , but it still remains moderate.

IV. CONCLUSION

We have developed an accurate model describing the interaction of ^{39}K atoms with two pulses in the counterintuitive order characteristic of STIRAP processes, coupled to a D_1 transition involving states with two values of the total angular momentum, namely, $F = 1$ and $F = 2$, in both the ground and excited manifolds. We have studied the efficiency of population transfer, through a four-photon process involving both pulses,

from the atomic state $F = 2, M_F = +2$ to another atomic state with different quantum numbers, $F = 1, M_F = 0$ (both states lying in the ground manifold).

We have found that the participation of more than one atomic state at each intermediate step of the multiphoton process prevents fulfillment of the so-called proportional couplings condition and there is no adiabatic-passage state. At the same time, the interaction of the fields with atomic states beyond the target state and the impossibility for the fields to be simultaneously on resonance with all intermediate steps of the four-photon process also negatively affect, through induced light shifts, the efficiency of the population-transfer process.

Nevertheless, we have also shown that, by scanning the frequencies of the two fields and going out of four-photon resonance, values can be found for which the atomic state can jump diabatically from one eigenstate of the Hamiltonian to another eigenstate through an avoided crossing and in this way efficiently reach the target state. The efficiency of the population transfer from the initial to the target state grows monotonically with fields amplitude and can reach very large values. It is also significantly robust against variations in the parameter values.

Scanning the frequency of the fields, as well as controlling the rest of pulse characteristics, is a task that could be performed in the laboratory. Thus, in principle, these results open the possibility for new atom optics, quantum optics, or nonlinear optics experiments in potassium and in similar atoms. In particular, they open the possibility to improve the efficiency of the two-photon laser system implemented in

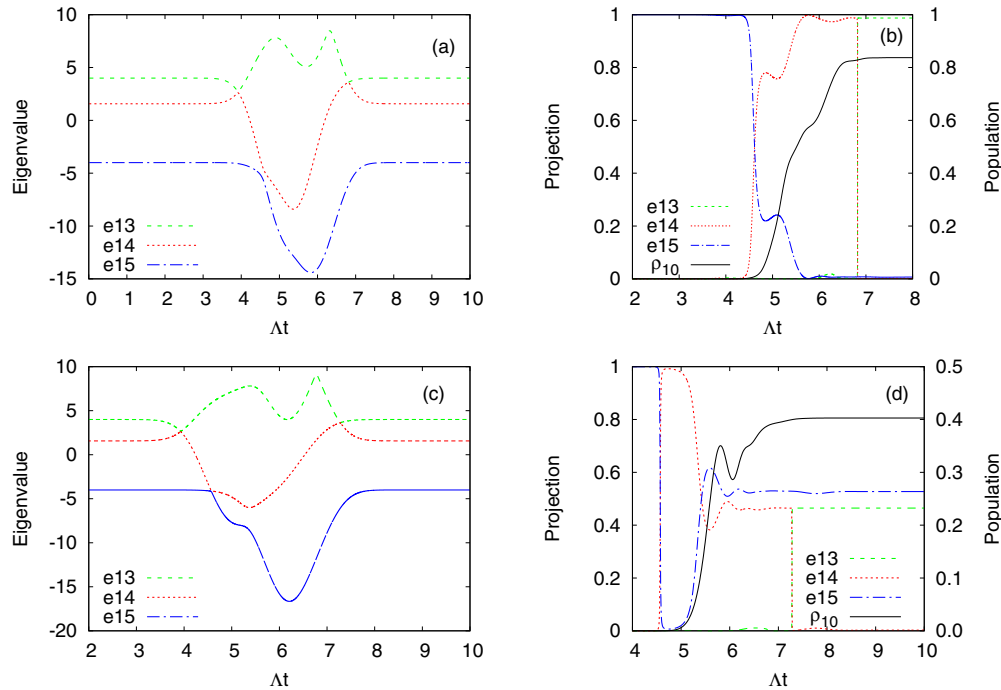


FIG. 12. (a) Most relevant Hamiltonian eigenvalues (denoted by e_{13} , e_{14} , and e_{15}) as a function of time, for point B' of Fig. 7, for which $\tau = 0.63$. (b) Corresponding projection (square component) of the exact atomic state on eigenstates e_{13} , e_{14} , and e_{15} (left vertical axis) and population of target atomic state 10, ρ_{10} . (c) and (d) Same as in (a) and (b), respectively, when the pulse delay τ is changed from 0.63 (point B') to 1.09 [see Fig. 11(a)]. In all cases the Stokes pulse has been centered at $\Delta t_c = 5$.

potassium in the past [23], which was based on a four-photon process similar to the one considered here. This, if successful,

could make experimental investigation of the *a priori* rich two-photon laser dynamics possible.

-
- [1] U. Gaubatz, P. Rudecki, S. Schieman, and K. Bergmann, *J. Chem. Phys.* **92**, 5363 (1990).
- [2] B. W. S. Nikolay V. Vitanov, A. A. Rangelov, and K. Bergmann, *Rev. Mod. Phys.* **89**, 015006 (2017).
- [3] N. Vitanov, B. Fleischhauer, B. Shore, and K. Bergmann, *Adv. At. Mol. Opt. Phys.* **46**, 55 (2001).
- [4] N. Vitanov, T. Halfmann, B. Shore, and K. Bergmann, *Annu. Rev. Phys. Chem.* **52**, 763 (2001).
- [5] K. Bergmann, N. V. Vitanov, and B. W. Shore, *J. Chem. Phys.* **142**, 170901 (2015).
- [6] K. Bergmann, H. Theuer, and B. Shore, *Rev. Mod. Phys.* **70**, 1003 (1998).
- [7] L. S. Goldner, C. Gerz, R. J. C. Spreeuw, S. L. Rolston, C. I. Westbrook, W. D. Phillips, P. Marte, and P. Zoller, *Phys. Rev. Lett.* **72**, 997 (1994).
- [8] L. Goldner, C. Gerz, R. Spreeuw, S. Rolston, C. Westbrook, W. Phillips, P. Marte, and P. Zoller, *Quantum Opt.* **6**, 387 (1994).
- [9] P. D. Featomb, G. S. Summy, J. L. Martin, H. Wu, K. P. Zetie, C. J. Foot, and K. Burnett, *Phys. Rev. A* **53**, 373 (1996).
- [10] V. Malinovsky and D. Tannor, *Phys. Rev. A* **56**, 4929 (1997).
- [11] P. Marte, P. Zoller, and J. L. Hall, *Phys. Rev. A* **44**, R4118 (1991).
- [12] B. W. Shore, K. Bergmann, J. Oreg, and S. Rosenwaks, *Phys. Rev. A* **44**, 7442 (1991).
- [13] J. Oreg, K. Bergmann, B. W. Shore, and S. Rosenwaks, *Phys. Rev. A* **45**, 4888 (1992).
- [14] P. Pillet, C. Valentin, R.-L. Yuan, and J. Yu, *Phys. Rev. A* **48**, 845 (1993).
- [15] A. Smith, *J. Opt. Soc. Am. B* **9**, 1543 (1992).
- [16] H. Theuer and K. Bergmann, *Eur. Phys. J. D* **2**, 279 (1998).
- [17] C. Valentin, J. Yu, and P. Pillet, *J. Phys. France II* **4**, 1925 (1994).
- [18] N. V. Vitanov, *Phys. Rev. A* **58**, 2295 (1998).
- [19] N. V. Vitanov, B. W. Shore, and K. Bergmann, *Eur. Phys. J. D* **4**, 15 (1998).
- [20] R. M. Godun, C. L. Webb, M. K. Oberthaler, G. S. Summy, and K. Burnett, *Phys. Rev. A* **59**, 3775 (1999).
- [21] C. L. Webb, R. M. Godun, G. S. Summy, M. K. Oberthaler, P. D. Featomb, C. J. Foot, and K. Burnett, *Phys. Rev. A* **60**, R1783(R) (1999).
- [22] D. J. Gauthier, *Progress in Optics* (Elsevier, Amsterdam, 2003), Vol. 45.
- [23] O. Pfister, W. J. Brown, M. D. Stenner, and D. J. Gauthier, *Phys. Rev. Lett.* **86**, 4512 (2001).
- [24] O. Pfister, W. J. Brown, M. D. Stenner, and D. J. Gauthier, *Phys. Rev. A* **60**, R4249(R) (1999).
- [25] D. J. Gauthier, Q. Wu, S. E. Morin, and T. W. Mossberg, *Phys. Rev. Lett.* **68**, 464 (1992).
- [26] B. Nikolaus, D. Z. Zhang, and P. E. Toschek, *Phys. Rev. Lett.* **47**, 171 (1981).
- [27] R. Vilaseca, M. C. Torrent, J. García-Ojalvo, M. Brambilla, and M. San Miguel, *Phys. Rev. Lett.* **87**, 083902 (2001).

- [28] J. L. Font, J. J. Fernández-Soler, R. Vilaseca, and D. J. Gauthier, *Phys. Rev. A* **72**, 063810 (2005).
- [29] J. J. Fernández-Soler, J. L. Font, R. Vilaseca, D. J. Gauthier, A. Kul'minskii, and O. Pfister, *Phys. Rev. A* **65**, 031803 (2002).
- [30] G. J. de Valcárcel, E. Roldán, J. F. Urchueguía, and R. Vilaseca, *Phys. Rev. A* **52**, 4059 (1995).
- [31] J. Zakrzewski, M. Lewenstein, and T. W. Mossberg, *Phys. Rev. A* **44**, 7746 (1991).
- [32] A. W. Boone and S. Swain, *Phys. Rev. A* **41**, 343 (1990).
- [33] S.-Y. Zhu and M. O. Scully, *Phys. Rev. A* **38**, 5433 (1988).
- [34] L. M. Narducci, W. W. Eidson, P. Furcinitti, and D. C. Eteson, *Phys. Rev. A* **16**, 1665 (1977).
- [35] A. Prokhorov, *Science* **149**, 828 (1965).
- [36] P. Sorokin and N. Braslau, *IBM J. Res. Dev.* **8**, 177 (1964).
- [37] J. Martin, B. W. Shore, and K. Bergmann, *Phys. Rev. A* **54**, 1556 (1996).
- [38] J. J. Fernández-Soler, J. L. Font, R. Vilaseca, D. J. Gauthier, and A. Kul'minskii, *Phys. Rev. A* **68**, 043824 (2003).
- [39] N. V. Vitanov and S. Stenholm, *Phys. Rev. A* **60**, 3820 (1999).
- [40] C. E. Carroll and F. T. Hioe, *Phys. Rev. Lett.* **68**, 3523 (1992).
- [41] G. Coulston and K. Bergmann, *J. Chem. Phys.* **96**, 3467 (1992).
- [42] I. R. Sola and V. S. Malinovsky, *Phys. Rev. A* **68**, 013412 (2003).
- [43] M. Weitz, B. C. Young, and S. Chu, *Phys. Rev. A* **50**, 2438 (1994).
- [44] S. Guérin, L. P. Yatsenko, T. Halfmann, B. W. Shore, and K. Bergmann, *Phys. Rev. A* **58**, 4691 (1998).
- [45] J. Martin, B. W. Shore, and K. Bergmann, *Phys. Rev. A* **52**, 583 (1995).
- [46] I. I. Boradjiev and N. V. Vitanov, *Phys. Rev. A* **81**, 053415 (2010).
- [47] J. Oreg, F. T. Hioe, and J. H. Eberly, *Phys. Rev. A* **29**, 690 (1984).
- [48] A. A. Rangelov, N. V. Vitanov, L. P. Yatsenko, B. W. Shore, T. Halfmann, and K. Bergmann, *Phys. Rev. A* **72**, 053403 (2005).
- [49] L. P. Yatsenko, N. V. Vitanov, B. W. Shore, T. Rickes, and K. Bergmann, *Opt. Commun.* **204**, 413 (2002).
- [50] M. P. Fewell, B. W. Shore, and K. Bergmann, *Aust. J. Phys.* **50**, 281 (1997).